Air Quality, Atmosphere & Health (2018) 11:649–663
https://doi.org/10.1007/s11869-018-0572-6

Incense powder and particle emission characteristics during and after burning incense in an unventilated room setting

Bojana Višić[1] · Eva Kranjc[1,2] · Luka Pirker[1] · Urška Bačnik[1] · Gašper Tavčar[1] · Srečo Škapin[1] · Maja Remškar[1]

Received: 10 January 2018 / Accepted: 28 March 2018 / Published online: 11 April 2018

Abstract

Despite being a recognized health hazard, burning incense remains in widespread use. A number of studies have investigated the emissions of air pollulants from incense burning, but less attention has been given to particle decay following incense burning. We have studied the elemental composition and indoor emission characteristics of incense sticks in terms of the size distribution and concentrations of fine particles. The results of chemical analysis and energy dispersive X-ray spectroscopy showed that the primary constituents of the emissions were $CaCO_3$ and SiO_2, together with lesser amounts of Mg, K, Al, Fe, and Cl. Analysis using a scanning mobility particle sizer revealed that the maximum total particle concentration at the end of the burning period was up to 30-fold higher than that of the initial background levels and that it remained elevated even 100 min after the incense sticks had been completely burned up. Emitted incense particles decayed in a biexponential manner, with particles of up to 100 nm in size decaying with lifetimes of several tens of minutes, while nanoparticles with diameters of 100–700 nm having lifetimes of > 100 min, as their removal mechanisms are slower. The peak particle size immediately following the end of incense burning was 85 nm, and this increased to 110 nm at 100 min after completion of burning. This result indicates that a high proportion of emitted particles can be inhaled into the alveolar region of the lung, where the potential for adverse health effects is the greatest. These findings provide a more detailed insight into particle decay mechanisms under conditions of low ventilation, with implications for human health.

Keywords Incense · Smoke · Size distribution · Nanoparticles · Nanoparticle decay

Introduction

Incense combustion has been identified as a significant source of indoor particulate matter (PM) and contaminant exposures due to its relatively widespread uses as an air freshener, insect repellent, and object of cultural expression and religious worship (Chuang et al. 2011, 2013; Cohen et al. 2013; Fang et al. 2003; Ho and Yu 2002; Huynh et al. 1991; Jetter et al. 2002; Lee and Wang 2004; Lin et al. 2007; Löfroth et al. 1991; Lung et al. 2003; Navasumrit et al. 2008; Ott and Siegmann 2006; See and Balasubramanian 2011; See et al. 2007; Stabile et al. 2012; Yang et al. 2007). Incense emissions are comparable or greaterr than cigarette smoke emissions, another significant polluter of indoor air quality (Cohen et al. 2013; Lee and Wang 2004; Löfroth et al. 1991; See and Balasubramanian 2011; Wang et al. 2006). Incense comes in many forms (e.g., cones, sticks, coils, powders, rocks) and can be composed of numerous materials, including resins, aromatic plant materials, essential oils, and synthetic chemicals (Jetter et al. 2002).

Despite its widespread appeal, incense smoke has been found to contain harmful substances as well as to have a number of adverse health impacts that are attributed to its inhalation and deposition. PM, a mixture of solid particles and liquid droplets suspended in air, is abundantly present in incense smoke (Chang et al. 2007; Jetter et al. 2002; Vu et al. 2017). For example, Yang et al. (2007) reported that most of the airborne PM emitted from nine different types of incense sticks was < 5.6 μm in diameter, with 95% of particles (by total weight) in this size range being < 1.0 μm ($PM_{1.0}$). Carcinogens (e.g., polycyclic aromatic hydrocarbons [PAHs], volatile organic compounds [VOCs] such as benzene

Electronic supplementary material The online version of this article (https://doi.org/10.1007/s11869-018-0572-6) contains supplementary material, which is available to authorized users.

✉ Bojana Višić
bojana.visic@ijs.si

[1] Jozef Stefan Institute, Jamova cesta 39, 1000 Ljubljana, Slovenia

[2] Jozef Stefan International Postgraduate School, Jamova cesta 39, 1000 Ljubljana, Slovenia

and 1,3-butadiene, and certain metals), suspected carcinogens (e.g., formaldehyde and acetaldehyde), irritants (e.g., acrolein and acetic acid), and allergens (e.g. geraniol) have also been detected in incense smoke (Bootdee et al. 2016; Ho and Yu 2002; Kuo and Tsai 2017; Kuo et al. 2016; Lui et al. 2016; Lung et al. 2003; Navasumrit et al. 2008). Ho and Yu (2002) found that fFormaldehyde and acrolein concentrations were in excess of World Health Organization (WHO) air quality guidelines in the interior and outside yard of a temple, as well as inside a home where incense was burned. In a similar study, Lee and Wang (2004) reported that all types of PM (< 10 μm in diameter [PM_{10}] and < 2.5 μm in diameter [$PM_{2.5}$]) and benzene emissions from ten types of incense exceeded the Recommended Indoor Air Quality Objectives for Office Buildings and Public Places in Hong Kong, while those for CO and formaldehyde were exceeded by seven and six of the tested incenses, respectively.

PM in the nanometer size range has a well-documented role in promoting pulmonary and cardiovascular disease due to its ability to enter the furthest (alveolar) regions of the lung (Vu et al. 2017). The formation of reactive oxygen species (ROS) from interference with cellular mechanisms and inflammation can lead to fibrosis and cancer in the long term (Brown et al. 2002; Cheng et al. 1995; Lewinski et al. 2009; Nel et al. 2006). Furthermore, due to its large surface area and high reactivity, PM readily binds with metal(loid)s and other pollutants in incense smoke, thereby increasing its oxidative capacity (Chuang et al. 2011, 2013). Not only is there exposure to incense PM through inhalation, but incense PM can also be deposited onto exposed skin (Hayakawa et al. 1987) and be ingested following deposition onto the surfaces of foods and drinks (e.g. if incense is burned to mask cooking odors) (Vance and Marr 2015). Incense PM has been found to cause dose-dependent oxidative damage in the plasmid scission assay (particularly in the presence of metal[loid[s, such as Cu) (Chuang et al. 2011) and mutagenicity in the Ames salmonella test (Löfroth et al. 1991). Regular (i.e., daily) domestic incense use has been associated with decreased weight (among boys, but not girls) and head circumference at birth (Chen and Ho 2016), decreased lung function among adolescents (Chen et al. 2017), and increased hypertension and blood pressure (especially among women) (Song et al. 2017).

Although PM measurements have often been conducted using units of mass per unit volume, particle number concentrations per unit volume of air have been recognized as a more effective indicator of potential harm (Hinds 2012). Currently, the European Union (EU) only sets a mass-based limit of 20 $\mu g/m^3$ for $PM_{2.5}$ over a 3-year averaging period (EU Directive/2008/50 2015; http://ec.europa.eu/environment/air/quality/standards.html). The characteristics of fine particle emissions during the burning of incense have been intensively studied (Chang et al. 2007; Ji et al. 2010; Lin et al. 2007; See and Balasubramanian 2011; See et al. 2007; Stabile et al. 2012; Yang et al. 2007), but fewer studies have focused on particle decay following incense burning under conditions of low ventilation (Cheng et al. 1995; Ji et al. 2010; Mannix et al. 1996). This information is relevant given the known fact that different aerosol size fractions exhibit different deposition characteristics, therefore affecting the relative level and duration of air pollution (Rim et al. 2012). Two separate studies have described particle decay following incense burning, but both reported the results in terms of mass per unit volume of air, with only limited information provided on the change in distribution and concentration of particle size with time (Cheng et al. 1995; Mannix et al. 1996). In a third study in which particle decay was also investigated, the focus was on the dispersion of emitted particles to surrounding rooms within a multi-room domestic setting (Ji et al. 2010). The primary aim of our study was, therefore, to investigate particle decay at a more detailed level in terms of the size distribution and concentration of nanoparticles with time before, during, and following the burning of incense.

In this study, the elemental composition and physical morphology of two types of scented Indian incense sticks, namely, "African Violet" ("AV") and "Strawberry" ("S"), were investigated in both the burned and unburned incence sticks using chemical analysis, X-ray diffraction (XRD), and scanning electron microscopy coupled to energy dispersive X-ray spectroscopy (SEM-EDS). The nanoparticle emissions produced during and following the burning period were investigated in terms of size and size-specific mass distribution and concentration using a scanning mobility particle sizer (SMPS) and a Dekati® low-pressure cascade impactor (DLPI; Dekati Ltd., Knoxfield, Australia). The implications of our findings for human exposure and health are also discussed.

Methods and materials

Incense burning protocol

Incense burning measurements were performed using the two different incense types chosen for this study, namely "African Violet" and "Strawberry" (Hem Corp., Mumbai, India; www.hemincense.com). These two incenses were chosen as they are the most common ones on the market and come from the same manufacturer, thus ensuring consistency and repeatability of the experiments. The measurements were carried out at varying distances from the measurement inlet (15, 100, and 300 cm). For each distance, three measurements were made (with nine measurements in total for each incense). Hence, particle number distributions and concentrations as a function of distance from the incense source could be determined. All measurements were completed in an empty room with dimensions of 2.7 (length) × 3.8 (width) × and 3.1 m

(height), making a total volume of 31.8 m^3. The room has one door and one wall of windows, as might be observed in a typical room of a residential dwelling (i.e., bedroom, office, or living room). The door and windows were closed during the measurements. In addition, the room was completely empty during the measurements, with no additional elements that could impact nanoparticles on the surfaces. The air exchange rate was not measured, but there was no detectable draft in the room as the windows were newly installed; the conditions for all measurements were roughly the same. The temperature and humidity for each measurement were recorded and are presented in Electronic Supplementary Material (ESM) Table 1S. After the background particle concentrations had been measured, a gas lighter was used to light each incense stick. It had been shown that this combustion source does not noticeably influence subsequent particle measurement readings. Each incense stick was allowed to burn to completion, followed by an additional measurement of the background particle concentrations to monitor the decrease in particle concentrations. After completion of the experiment, the room was vented overnight, and the background levels tested before new measurements were made. The shortest and the longest burning times were 39 and 57 min, respectively. In the tables presented, the measurements are labeled by the incense name (S or AV), distance from the inlet (15, 100, or 300 cm), and the trial run (1, 2, or 3).

Distribution and concentration

The distributions and concentrations of nanoparticles in the emissions from the burning incense were measured with a SMPS (model 3638 L85; TSI Co., Shoreview, MN, USA) equipped with an attachable desiccator, soft X-ray neutralizer, long differential mobility analyzer (DMA), and a water condensation particle counter (WCPC; model 3785; TSI). This model measures particle size distribution from 15 to 700 nm based on the electrical mobility of the particles. The DMA first separates the nanoparticles according to size, following which the WCPC counts them. The measurements were performed as successive 3-min scans.

Additional information on the mass distribution and content of the emitted incense in the air was obtained using a multi-stageDLPI which collects particles using 13 diameter-selected filters varying from 30 nm up to 10 μm. As such, once the initial mass of the filters is known, the mass of the emitted particles can be obtained in a size-selected manner. The DLPI was operated alongside the TSI SMPS for 4 to 10 h. The same setup was used by Remškar et al. (2015) to measure the size distribution of nanoparticles emitted from sparklers.

Chemical analysis

The amounts of carbon, hydrogen, and nitrogen were determined by elemental analysis using a vario EL cube elemental analyzer (Elementar Co., Langenselbold, Germany). The samples for the chemical analysis were decomposed by the alkali fusion method. The amounts of aluminum and iron were determined by inductively coupled plasma–mass spectrometry (ICP-MS), calcium was quantified by complexometric titration, while silicon was quantified spectrophotometrically.

XRD was performed using a D4 Endeavor diffractometer (Bruker AXS GmbH, Karlsruhe, Germany) at room temperature. A quarzt monochromator Cu Ka1 radiation source ($\lambda = 0.1541$ nm) and a Sol-X energy dispersive detector were used. The angular range (2ϑ) was chosen to range from 5° to 75°, with a step size of 0.02° and collection time of 4 s. The unburned (pure) incense was prepared for chemical analysis by removing the contents of the stick with a knife, while the remaining ash from the burned incense was collected and measured.

For the SEM-EDS analysis, burned and unburned incense samples were attached to double-sided carbon tape and sputter-coated with Au (particle size: approx. 10 nm) using an SCD 005 cool sputter coater (BAL-TEC GmbH, Leica Microsystems, Wetzlar, Germany).

Results and discussion

Incense chemical analysis

Results of the elemental analysis indicate the presence of Ca, Si, Fe and Al together with different organic compounds in the unburned material (Table 1). X-ray powder diffraction and chemical analysis revealed that $CaCO_3$ and SiO_2 were the major inorganic components in both samples; these were probably added as a filler (Yang et al. 2006). Organic compounds evaporate and decompose during the slow combustion of the incense stick, with a mass reduction of 86.5% for "AV" and 60.2% for "S" incense sticks, resulting in the content of inorganic compounds increasing (Table 1). $CaCO_3$ is decarboxylated during the combustion and basic CaO is formed, resulting in further absorption of acidic CO_2 from the air, making the speciation difficult to identify. Fang et al. (2003) reported that the presence of C in incense sticks decreases the amount of C particles. In order to avoid the effect of CO_2 absorption, the chemical analysis was performed immediately after decomposition, and all the samples were kept in a desiccator. The constituents of the ash obtained after the combustion were SiO_2, CaO, and $CaCO_3$, with small quantities of Al_2O_3, Fe_2O_3, and $CaSO_4$.

Figure 1 shows the XRD spectra of "S" (Fig. 1a) and "AV" (Fig. 1b) incenses, both unburned (red line) and burned (black

Table 1 Elemental composition of the two incenses before and after combustion

Element	S	S, burned	AV	AV, burned
Ca	9.8	12.5	2.2	12.5
Al	0.41	5.36	0.77	5.36
Fe	0.17	2.43	0.242	2.43
Si	7.9	17.2	3.5	24.36
C	44.96	6.02	51.15	6.02
H	3.66	0.25	4.76	0.25
N	0.32	0.03	0.36	0.03
S	0.03	0.13	0.04	0.13
Cl	0	0	0	0
Sum	67.25	51.08	63.02	51.08

Values in table are presented as wt.%

S, "Strawberry" incense; AV "African Violet" incense

line). For both incenses, the burned sample was more sharp, since the leftover powder was more crystalline due to all moisture having been removed by burning. All of the peaks of both incenses were preserved after burning, with some relative changes in intensities. This effect can be attributed both to changes in the chemical composition following burning and to changes in the orientation of the crystallites in the samples.

For the "S" incense before burning, the XRD spectrum corresponds predominantly to the mixture of $CaCO_3$ (ICSD number 024-0027) and SiO_2 (ICSD number 083-0539), with traces of Fe_2O_3 (ICSD number 024-002) and $CaSO_4$ (ICSD number 003-0163). Upon combustion, in addition to $CaCO_3$ and SiO_2, CaO becomes a dominant species (ICSD number 037-1497). "AV" has a more complicated pattern, with $CaCO_3$, SiO_2, and CaO as the most prominent compounds, together with small additions of Al_2O_3 (ICSD number 008-0013), Fe_2O_3, and $CaSO_4$. All of these peaks were preserved after burning. These spectra are depicted in more detail in ESM Fig. 1S. It should be noted that various VOCs (such as nicotinic acid $C_6H_5NO_2$ [ICSD number 049-2089] or malononitrile $C_3H_2N_2$, [ICSD number 033-1737]) can be a match, but they overlap with the much stronger peaks of $CaCO_3$ and SiO_2. Many of those VOCs have been previously identified in incense smoke (Zhou et al. 2015).

Figures 2 and 3 present SEM images of both the burned and unburned incenses, together with a representative EDS image. The EDS analysis corresponding to Fig. 2c and Fig. 2f is summarized in Table 2 for the "S" incense; similarily, the EDS analysis corresponding to Fig. 3c and Fig. 3f is summarized in Table 3 for the "AV" incense. Therefore, "F2 C1" in Table 2 Fig. 2c, position 1.

The EDS analysis shows that a variety of elements are present inside the incense, with C, O and Ca being the most abundant. Smaller amounts of Si, Mg, K, Al, and Cl were also detected. Although the presence of Cl was confirmed, this element occurred only sporadically, explaining why it was not detected in the elemental analysis. The exceptionally high amount of O may be attributed to the formation of hydrates. If the incense powder is exposed to ambient conditions, it can absorb water, forming hydrates. It appears that the burning process reduces the size of the material blocks, leaving behind a powder ash. While the bigger blocks have a fairly uniform composition, the powder form is much more complex and contains many different elements.

Variations in the elemental content between different brands and types of incense are to be expected. Nonetheless, the results in this study generally concur with previous findings, which have identified, on average, Ca as a dominant element in incense, along with lesser amounts of Al, Fe, Mg, and K (Chuang et al. 2011; Lin et al. 2007). However, See and Balasubramanian (2011) found Al and Fe to be the dominant metals in six types of unburned incense, while Chuang et al. (2013) identified relatively large concentrations of Zn and Cu in two of the three types of tested incense they tested, with Fe

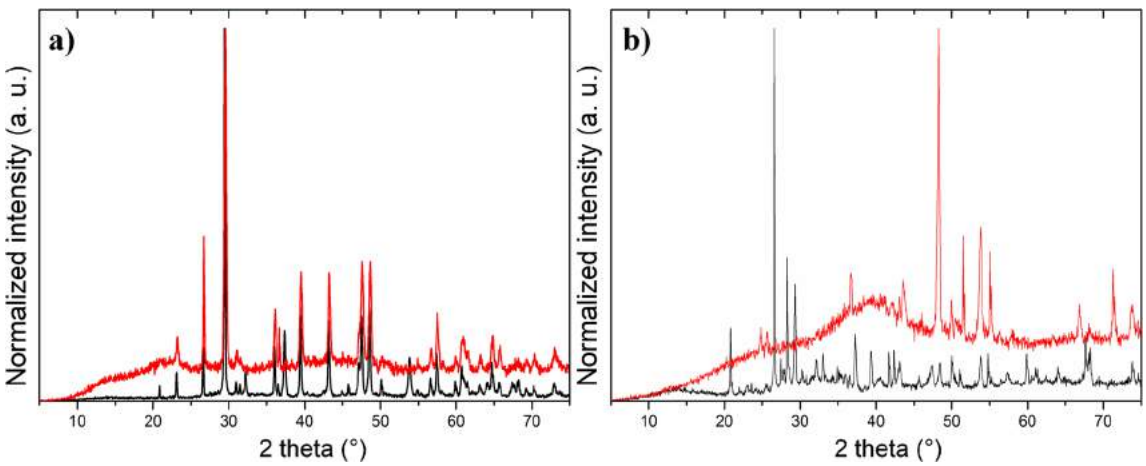

Fig. 1 X-ray diffraction spectra of "Strawberry" (**a**) and "African Violet" (**b**) incenses, both unburned (red line) and burned (black line)

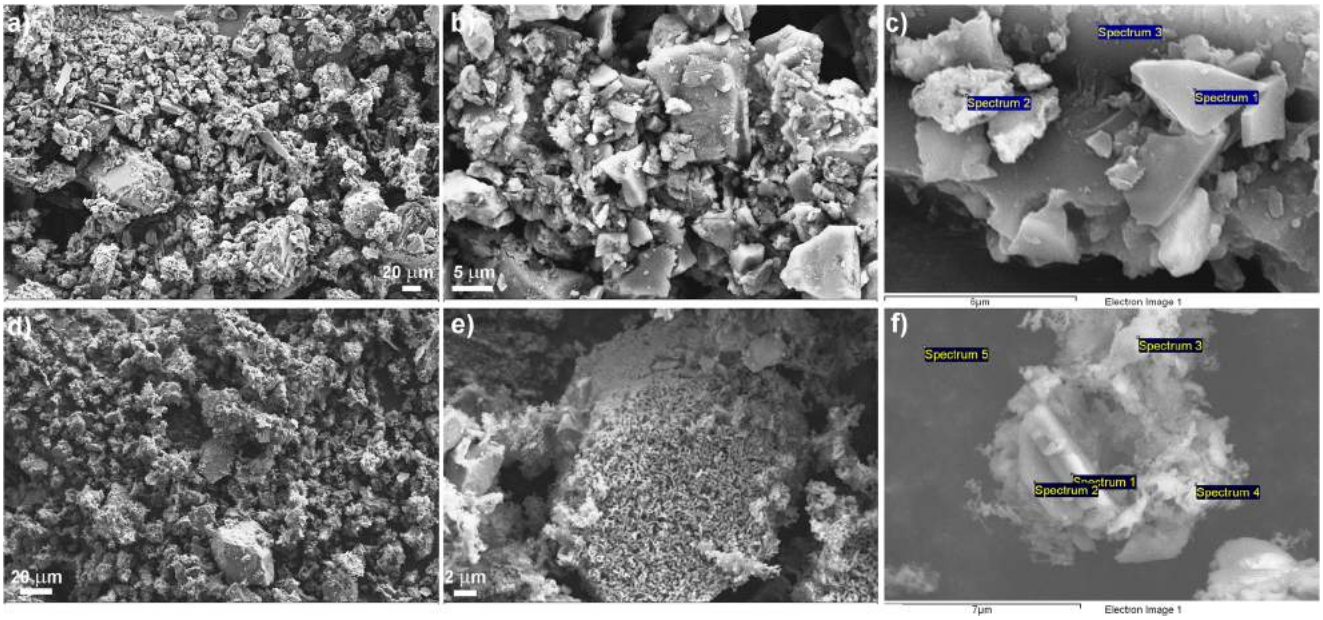

Fig. 2 Scanning electron microscopy images of "Strawberry" incense. Top panel: Unburned incense; bottom panel: burned material. **c**, **f** Representative images for energy dispersive X-ray spectroscopy (EDS) analysis

falling below the limit of detection for all three types of incense. Although we did not identify the relationship between elemental content and emission factors in our study, previous investigations have shown that an increased metal content in unburned incense is associated with decreased PM emissions, while increased C content is associated with increased PM emissions (See and Balasubramanian 2011). In the case of C content, a 1% decrease led to a 2.6 mg/g decrease in emitted material (Lin et al. 2007)

Size distributions and concentrations of emitted incense nanoparticles

The size distributions and total nanoparticle concentrations (TPC) of the "S" and "AV" incenses released 100 cm from the measurement inlet are shown in Figure 4. The stages at which the initial background particle concentrations were measured, as well as the times when the incense was lit and when it released maximum emissions (close to when the

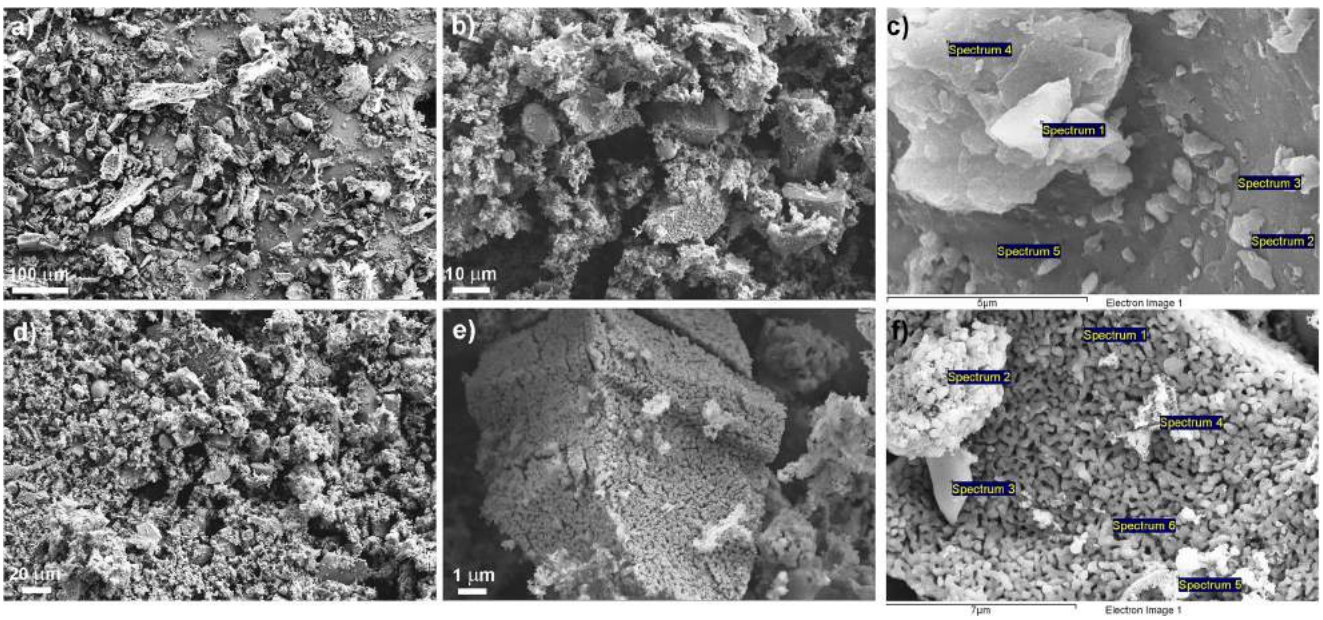

Fig. 3 Scaning electronic microscopy images of "African Violet" incense. Top panel: U unburned incense; bottom panel: burned material. **c**, **f** Representative images for the EDS analysis

Table 2 Energy dispersive X-ray spectroscopy analysis of "Strawberry" incense corresponding to images in Fig. 2c, f

Fig. 2c, f images[a]	C	O	Mg	K	Al	Si	Cl	Ca	Fe	P
F2 C1	81.2	18.1		0.1		0.1		0.5		
F2 C2	68.9	28.8	0.2	0.2	0.3	0.4	3.9	1	0.1	
F2 C3	85.8	14		0.1				0.1		
F2 F1	29	59.7						11.3		
F2 F2	26	59						15		
F2 F3	27	63				0.2		9.3		
F2 F4	25.6	59.6	1.1	1.7	1.8	2.1	0.4	7.1		0.5
F2 F5	21	79								

Values are given in atomic %

[a] First F2 refers to Fig. 2; C1–C3 and F1–F5 refer to Fig. 2 part c, positions 1–3 and Fig. 2 part f, positions 1–5, respectively

incenses burned out) are clearly visible from the plots. During each burning cycle, the incense was lit following a background measurement period. During burning, the particle concentration kept increasing with time, reaching a maximum concentration just before the incense burned out. Figure 4 contains measurements labeled as S100-2 and AV100-2 in Tables 4 and 5, referring to "Strawberry" and "African Violet" incenses, respectively, at the incense distance of 100 cm from the inlet. Two-dimensional (2D) plots for each of the 18 measurements are presented in ESM Figs. 2S and 3S.

In this specific measurement of the "S" incense at 100 cm from the inlet, the TPC of the background before the burning of incense commenced was 8×10^3 particles/cm^3 while the maximum measured concentration was 2.2×10^5 particles/cm^3. Therefore, burning of the "S" incense stick resulted in an almost 30-fold increase in the particle concentration with respect to the background levels. Specifically, the first scan after lighting the incense stick (after 3 min) already showed a fourfold increase in particle concentration. Furthermore, even 100 min after the incense stick had burned out, the total particle concentration did not return to the initial levels, remaining sixfold higher than the initial background concentrations at the time. Similar trends were observed for the "AV" incense stick, with the initial background levels being 12×10^3 and the maximum measured concentration being 2.1×10^5 particles/cm^3, or almost 20-fold higher than the initial background concentrations. Similarly, after 100 min, the background concentration was fourfold higher than at the initial point of the measurement. These results are summarized in Tables 4 and 5 for "S" and "AV" incenses, respectively. In other studies, increases in TPC from background levels have ranged from three- to fivefold times higher (Chang et al. 2007; Ji et al. 2010) to more than ninefold higher (Lung et al. 2003). This variation can be attributed to different experimental burning periods (shorter burning periods result in less emitted PM) and to differences in the combusted mass (with greater mass combustion resulting in higher concentrations of emitted PM) (Kuo et al. 2016; Lin et al. 2007; Mannix et al. 1996).

Table 3 Energy dispersive X-ray spectroscopy analysis of "African Violet" incense corresponding to images shown in Fig. 3c, f

Fig. 3c, f images[a]	C	O	Mg	K	Al	Si	Cl	Ca
F3 C1		96.2						3.8
F3 C2		93.1		3.6		3.3		
F3 C3		92		3.7				4.2
F3 C4		95.3		3				1.7
F3 C5		72.9					27.1	
F3 F1	9.3	44.4						46.3
F3 F2	25.1	73.7	1.2					
F3 F3		46.7	1.1	3.8	7.6	22.1		18.7
F3 F4	27.5	69.2	2.9	0.4				
F3 F5	33.2	64.9	1		0.3	0.6		
F3 F6	31.4	68.6						

Values are given in atomic %

[a] First F3 refers to Fig. 3; C1–C5 and F1–F6 refer to Fig. 3 part c, positions 1–5 and Fig. 3 part f, positions 1–6, respectively

The 2D plots (Fig. 4) show that the highest particle concentration on average is in the 60- to 100-nm diameter range during incense burning. This is also shown in Fig. 5, where the particle concentration over the course of the measurement period is plotted for the selected nanoparticle sizes (15, 50, 80, 200, and 685 nm). For the smallest measured particle size of 15 nm, the concentration maximum appears at the time when the incense is lit, with the concentration falling immediately after lighting and quickly reaching the initial background levels. This trend is observed for particles up to 30 nm in diameter and has been previously attributed to aggregation, which readily occurs at high particle concentrations (>20,000 particles/cm^3) (Cheng et al. 1995; Cohen et al. 2013). Aggregation is especially favored among smaller particles (< 50 nm) due to the presence and influence of Brownian motion and van der Waals forces (Rim et al. 2012). For particles with a diameter of > 30 nm, the concentration increases steadily until the incense burns out, reaching maximum concentrations for particles around 70–80 nm in diameter. The total concentration drops off significantly as the particles reach sizes of > 150 nm, while the concentrations of particles ≥ 300 nm in diameter are consistent with background levels.

Across most studies conducted to date, the highest particle concentration of emitted incense particles has been in the size range of approximately 70–180 nm (Chang et al. 2007; Ji et al. 2010; See et al. 2007; Vu et al. 2017). However, in their study, Jetter et al. (2002) detected the highest concentration of particles in the 30- to 60-nm size range for 23 different types of incense. This result was likely due to the design of the testing chamber. It has been shown that variations in the peak particle size are in

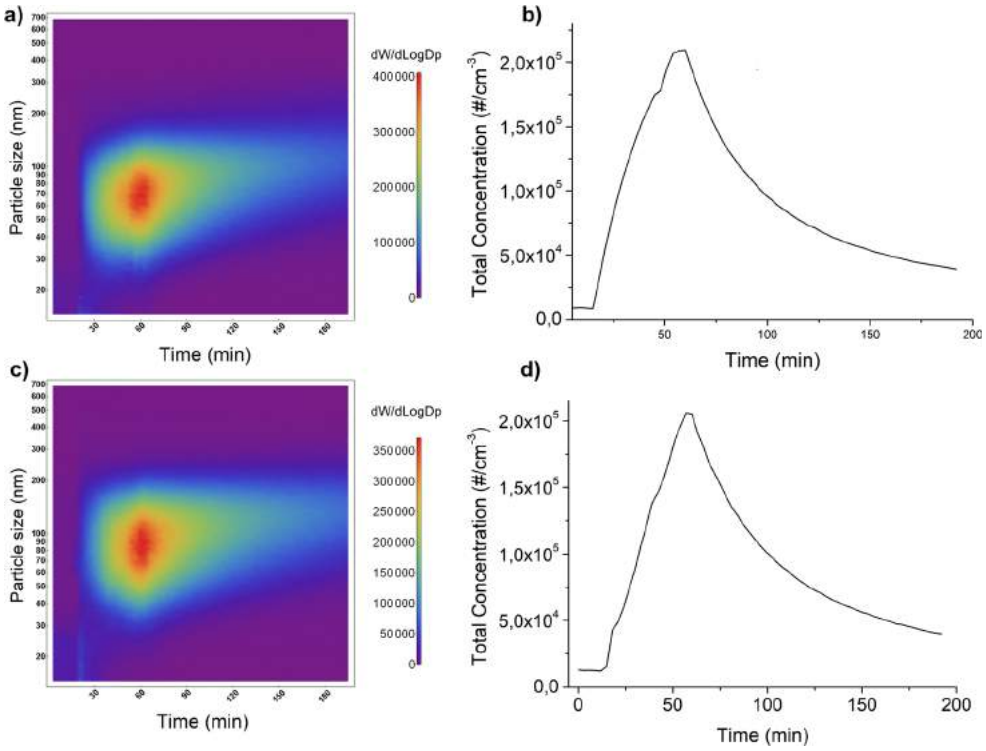

Fig. 4 **a**, **c** Nanoparticle distribution plots given as diameter (nm) versus time for "Strawberry" (**a**) and "African Violet" (**c**) incenses, respectively. **b**, **d** Total nanoparticle concentration (number of particles/cm^3) evolution for "Strawberry" (**b**) and "African Violet" (**d**) incenses, respectively. In both cases, the incense stick was positioned 100 cm from the measurment inlet

general mostly related to the degree of ingredient milling (Chang et al. 2007), with finer milling being associated with higher concentrations of smaller particles from incense burning (See et al. 2007). Other factors, such as testing room/chamber size, temperature, and humidity, have been found to have a negligible effect on the count median diameter and size distribution of emitted incense particles (Chang et al. 2007).

The mass of the incense together with the combusted mass (i.e., the mass of the particles emitted into the air, which was calculated by subtracting the mass of the burnt incense from that of the unburnt incense) and the burning duration are summarized in Tables 4 and 5 for "S" and "AV" incenses, respectively. Note that this measurement was conducted differently from the method used for the elemental analysis. In the latter, only the incense powder was used (i.e., scraped from the stick), while for this analysis the stick was burned as well, as is the case in conventional usage. The results suggest that the mass of the incense is not the only parameter governing the burning dynamics; other factors may be shape irregularities and environmental conditions.

The burning duration together with the total particle concentration for two time periods are summarized in Tables 6 and 7 for "AV" and "S" incenses, respectively. The first time period encompasses the burning period of the incense and the second time period comprises the first 60 min following the

Table 4 Physical and emission characteristics of "Strawberry" incense

Trial run[a]	Incense mass (g)	Combusted mass (g)	Burning duration (min)	Background TPC (particles/cm^3)	Maximum TPC (particles/cm^3)
S15-1	1.26	0.97	48	0.9×10^4	2.4×10^5
S15-2	1.08	0.81	45	0.8×10^4	2.6×10^5
S15-3	1.03	0.79	45	0.5×10^4	2.4×10^5
S100-1	1.23	0.93	51	0.5×10^4	2.2×10^5
S100-2	1.09	0.75	35	0.8×10^4	2.1×10^5
S100-3	1.23	0.84	45	0.8×10^4	2.2×10^5
S300-1	1.1	0.8	57	0.8×10^4	1.6×10^5
S300-2	1.17	0.9	57	0.4×10^4	1.9×10^5
S300-3	1.23	0.96	54	0.7×10^4	2.1×10^5

TPC, Total nanoparticle concentration

[a] S refers to "Strawberry incense; 15, 100, 300 refer to distance from the inlet (15, 100, or 300 cm, respectively); 1, 2, 3 refer to the trial run

Table 5 Physical and emission characteristics of "African Violet" incense

Trial run[a]	Incense mass (g)	Combusted mass (g)	Burning duration (min)	Background TPC (particles/cm^3)	Maximum TPC (particles/cm^3)
AV15-1	0.98	0.83	42	0.4×10^4	2.2×10^5
AV 15-2	1.19	1.03	45	0.8×10^4	2.6×10^5
AV 15-3	1.12	0.97	48	1.1×10^4	2.9×10^5
AV 100-1	0.94	0.81	42	1.1×10^4	2.1×10^5
AV 100-2	0.99	0.87	45	1.2×10^4	2.1×10^5
AV 100-3	0.87	0.73	39	0.9×10^4	2.1×10^5
AV 300-1	0.89	0.74	36	0.5×10^4	1.7×10^5
AV 300-2	1.00	0.85	39	1.7×10^4	1.9×10^5
AV 300-3	0.94	0.81	36	0.7×10^4	2.1×10^5

[a] AV refers to "African Violet incense; 15, 100, 300 refer to distance from the inlet (15, 100, or 300 cm, respectively); 1, 2, 3 refer to the trial run

end of incense burning. The correlation between the burning time and the TPC during both periods is very good. Nevertheless, a better correlation is achieved when TPC is compared with the combusted mass, as shown in Fig. 6**.** It can be observed that TPC increases with increasing combusted mass and that this parameter is more influential than the distance from the inlet. Previous researchers have also found that combusted mass is a significant factor affecting PM emissions (Lin et al. 2007; Mannix et al. 1996).

The evolution of the TPC (number of particles/cm^3) with time is shown in Fig. 7. The nanoparticle concentration was observed to decrease following biexponential decay after the burning period. The shorter lifetime was in the range of several tens of minutes, while the longer lifetime was > 100 min. The measured data (normalized with respect to the maximum TPC and with the zero time set at the point when the incense burned out) together with a biexponential function fit are shown in Fig. 7b, d so that the settling of the nanoparticles could be monitored. The plots for all 18 measurements are presented in ESM Fig. 4S. The R^2 for all the spectra were > 0.99. The physical properties of aerosols, including their dynamic behavior, is determined by particle size that is classified into three modes (Lagzi et al. 2013; Nazaroff 2004). Aerosol particles with diameters of < 100 nm constitute ultrafine, nucleation mode particles whose lifetimes are shorter due to their coagulation or random impaction on surfaces. The second mode observed by this detector is the accumulation mode, comprising particles with sizes of up to 1 μm. These nanoparticles have less efficient removal mechanisms and therefore have longer lifetimes. They can also be formed by the clustering of smaller particles and condensation of vapors onto existing particles. The third, coarse mode, comprises particles that are > 1μm; we did not observe such particles in our measuring system since the impactor removes particles of this size. Therefore, we can attribute the two time constants to the settling time of the two different nanoparticle modes: ultrafine and accumulation (Nazaroff 2004). Particle lifetimes increase with increasing distance of the incense stick from the inlet due to increased particle size from coagulation as the particles travel towards the impactor. Therefore, the concentration of particles in the size range of 60–100 nm is much higher when the incense stick is placed 15 cm, rather than 300 cm, from the measurement inlet. Various modeling techniques for studying indoor particle dynamics have been reported (Nazaroff 2004; Zhang and Chen 2006; Zhou et al. 2017; Zhuang et al. 2017). Some of the main parameters governing the modeling are ventilation supply, direct emissions of the particles, surface deposition, and mixing and resuspension of the particles. Therefore, deciphering the exact decay mechanisms requires an exacting control of all these external parameters, which was

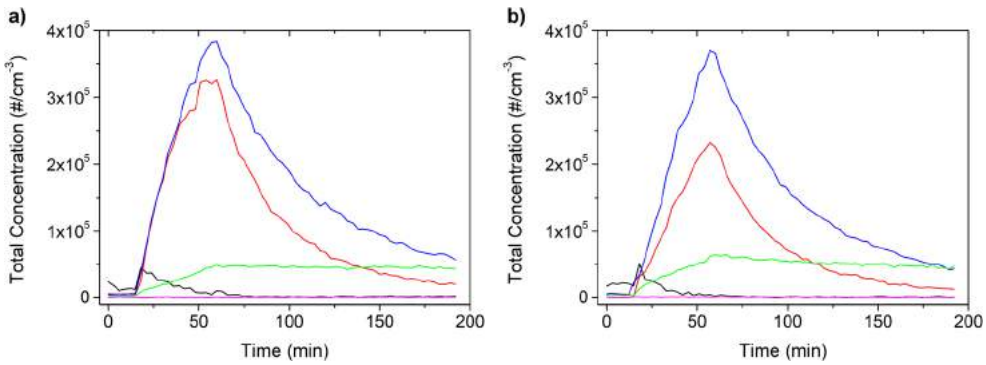

Fig. 5 Comparison of total concentration dynamics for particle sizes of 15 nm (black), 50 nm (red), 80 nm (blue), 200 nm (green) and 685 nm (pink) of "Strawberry" (**a**) and "African Violet" (**b**) incenses

Table 6 Burning duration and total particle concentration for the total burning period and the 60 min post-burning period, as well as biexponential time constants for "Strawberry" incense

Trial run[a]	Burning duration (min)	TPC during burning (particles/cm^3)	TPC at 60 min post-burning (particles/cm^3)	Time constants (min)
S15-1	48	6.7×10^6	8.8×10^6	8, 66
S15-2	45	4.9×10^6	7.2×10^6	20, 98
S15-3	45	4.5×10^6	6.8×10^6	5, 90
S100-1	51	6.0×10^6	7.8×10^6	22,.112
S100-2	35	5.7×10^6	8.2×10^6	23, 103
S100-3	45	5.8×10^6	8.5×10^6	28, 133
S300-1	57	5.6×10^6	6.0×10^6	33, 151
S300-2	57	6.0×10^6	6.6×10^6	41,.155
S300-3	54	6.7×10^6	7.8×10^6	21,.92

[a] S refers to "Strawberry" incense; 15, 100, 300 refer to distance from the inlet (15, 100, or 300 cm, respectively); 1, 2, 3 refer to the trial run

beyond the scope of our study. Nevertheless, the biexponential fitting of data, although a simplified method, appears to match the experimental data at a good level. Given the generally close similarity of the emission characteristics of burning incenses across different studies (particularly in terms of predominant fine particle emissions), we would expect to find similar particle decay patterns under the varied conditions of our experimental setup (i.e., so long as low ventilation is maintained) (Chang et al. 2007; Jetter et al. 2002; Ji et al. 2010; See et al. 2007; Vu et al. 2017; Yang et al. 2007).

Our results show a slight distance-dependent effects on the size distribution and concentration of the emitted particles. The TPC was found to be higher with decreasing distance to the measurement inlet, primarily due to higher concentrations of particles in the 60- to 100-nm size range. This observation is consistent the emitted PM not having as far to travel before reaching the measurement inlet and, therefore, nucleation mode particles did not coagulate to as significant a degree as those emitted from burning incense located further from the measurement inlet. Similar observations were reported in a similar study, in which incense particle emissions were measured at varying distances from a measurement inlet under conditions of low ventilation in a room setting (Chang et al. 2007; Lung et al. 2003).

In a number of related studies, exponential decay was clearly demonstrated in graphs depicting TPC decrease with time, but this phenomenon was not labeled as such and not described (Cohen et al. 2013; Ji et al. 2010; See et al. 2007). In two other studies, particle decay was examined, but because the results were obtained and presented in units of mass per unit volume of air, it was not possible to discern the size- and concentration-dependent mechanisms responsible for the decrease in TPC (Cheng et al. 1995; Mannix et al. 1996). In yet another study, particle decay was examined primarily in terms of particle dispersion to adjacent rooms within a multi-room house setting (Ji et al. 2010).

In our study, we show that under conditions of low ventilation, the TPC remains approximately sixfold higher even 100 min after the completion of incense burning. This finding is consistent with the fact that accumulation mode particles comprise the main fraction of the TPC. It

Table 7 Burning duration and total particle concentration for the total burning period and the 60 min post-burning period, as well as biexponential time constants for "African Violet" incense

Trial run[a]	Burning duration (min)	TPC during burning (particles/cm^3)	TPC for 60 min (particles/cm^3)	Time constants (min)
AV15-1	42	4.6×10^6	7.7×10^6	17, 113
AV 15-2	45	6.3×10^6	9.4×10^6	18, 110
AV 15-3	48	6.4×10^6	9.1×10^6	25, 116
AV 100-1	42	4.1×10^6	7.1×10^6	23, 82
AV 100-2	45	4.4×10^6	7.0×10^6	37, 148
AV 100-3	39	4.4×10^6	7.7×10^6	19, 90
AV 300-1	36	3.7×10^6	6.9×10^6	20, 101
AV 300-2	39	3.9×10^6	6.8×10^6	16, 75
AV 300-3	36	3.9×10^6	7.5×10^6	30, 130

[a] AV refers to "African Violet" incense; 15, 100, 300 refer to distance from the inlet (15, 100, or 300 cm, respectively); 1, 2, 3 refer to the trial run

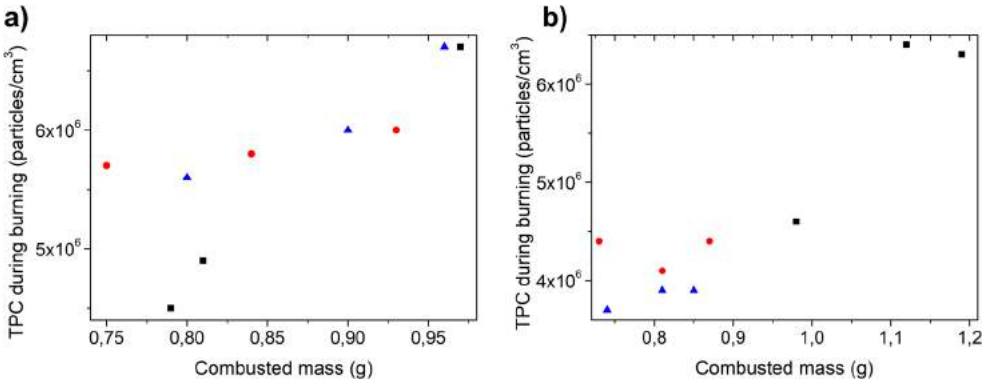

Fig. 6 Total nanoparticle concentration (*TPC*; number of particles/cm^3) as a function of the combusted mass for "Strawbery" (**a**) and "African Violet" (**b**) incenses. Black squares, red circles, and blue triangles correspond to nanoparticle concentrations counted when the incense was 15, 100, and 300 cm, respectively, from the measurement inlet

is difficult to compare our findings with those from other studies due to differences in incense type, burning duration, and ventilation rate. Complete particle decay has been found to take place in as little as 40 min (See et al. 2007) and in as much as 1–2 h (Ji et al. 2010) and in > 6 h (Lung et al. 2003). Many factors influence particle decay, including surface deposition from sedimentation, diffusion, and impaction (e.g., walls, floors, and other available surfaces), particle agglomeration, and changes in particle mass due to the evaporation and condensation of volatile components (Cheng et al. 1995; Mannix et al. 1996). Generally, the TPC decreases much more quickly under conditions of high ventilation due to increased surface deposition (Cheng et al. 1995). In one study, ventilation decreased PM_{10} concentrations by approximately ninefold9 times in comparison to unventilated conditions (Lung et al. 2003).

Particle size distributions, depicted in Fig. 8, are shown for selected time points during and after the burning period. The chosen time points include the background period prior to the incense being lit (T1, black), the first measurement after lighting the incense (T2, red), 15 min into the burning period (T3, blue), burnout of the incense (T4, cyan), 15 min after burnout (T5, pink), 1 h after burnout (T6, green). It can be seen that throughout the burning period that the peak particle size (maximum nanoparticle concentration) varies only about 5 nm (averaging around 85 nm for "AV" and 80 nm for "S"). When the burning process is over, the peak can be seen to shift to larger sizes (by approximately 25 nm), indicating that nanoparticles undergo agglomeration as they are settling. Furthermore, the pink line representing the distribution at 15 min after the burnout shows that the peak does not shift significantly, confirming that this time period is not sufficiently long for particle agglomeration.

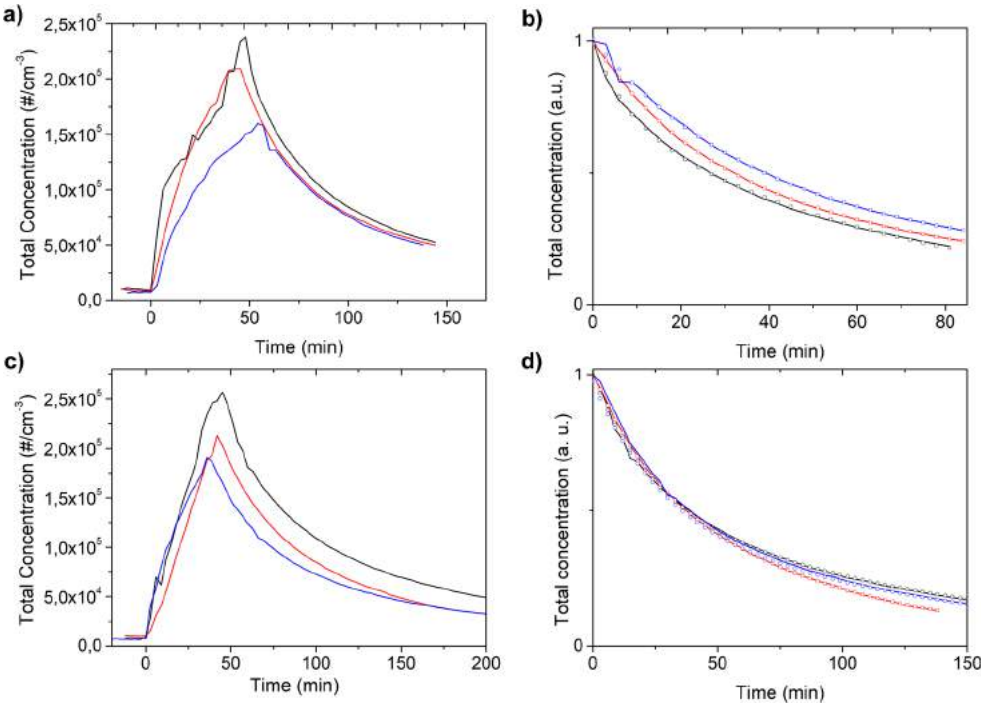

Fig. 7 **a**, **c** Evolution of total nanoparticle concentration (number of particles/cm^3) of "Strawberry" (**a**) and "African Violet" (**b**) incenses, respectively. **b**, **d** Normalized data (line) fitted to a biexponential function (circles) for "Strawberry" (**b**) and "African Violet" (**d**) incenses, respectively. Black lines, red lines, blue lines correspond to nanoparticle concentrations counted when the incense was 15, 100, and 300 cm, respectively, from the measurement inlet. *a.u.* Arbitrary units

Size-specific mass distribution of emitted incense particles

Information on the size-specific mass distribution of particles emitted during incense combustion was obtained using a DLPI. In the case of "S" incense, the total collected mass after 350 min of measurement was 0.854 mg. By weighing the filters individually, we found that nanoparticles (diameters ranging from 30 to 100 nm) amounted to 0.416 ± 0.1 mg, or 50 ± 10% of the total mass of the emitted particles; particles with sizes of 100–1000 nm amounted to 0.378 ± 0.1 mg, or 40 ± 10% of the total mass of the emitted particles; and particles in the diameter range from 1 to 10 μm constituted only 0.6 ± 0.1 mg, or 7 ± 10% of the total mass.

For "AV" incense, the total collected mass after 500 min of measurements was 1.422 mg. For this incense, nanoparticles (up to 100 nm in diameter) amounted to 0.349 + 0.1 mg, or 25 ± 10% of the total mass of emitted particles; particles in the 100- to 1000-nm range constituted 0.998 ± 0.1 mg (70 ± 10% of total mass of emitted particles); and particles in the range of 1–10 μm amounted to only 0.075 ± 0.1 mg (5 ± 10% of total mass of emitted particles). These observations are consistent with the total nanoparticle concentration evolution analysis which implied that nanoparticles larger than a few microns in size were not present. These results are in close agreement with a previous study which found that among the fraction of emitted incense particles of < 5.6 μm in diameter, 95% (by mass) were < 1.0 μm in diameter (Yang et al. 2007).

The filters with the collected material were subsequently analyzed with EDS in SEM, as the amount of material per filter was not sufficient for other methods such as XRD. In Fig. 9 SEM images of collected particles from the DLPI are shown. Particle diameters range from a few micrometers down to 20 nm. The smallest nanoparticles usually agglomerate into micrometer-sized particles, as seen in Fig. 9a. The EDS analysis is summarized in Table 8 and shows that most of the particles are made from C, but other elements can also be found. An Al substrate is used in the DLPI; therefore, the Al concentration cannot be determined from EDS measurements. Our finding that emitted incense particles were predominantly carbonaceous particles containing small proportions of metal(loids) is consistent with the findings of previous studies (Chuang et al. 2013; Chuang et al. 2011; See and Balasubramanian 2011). It has been found that emitted particles may also be composed of liquids, which solidify prior to coagulation with surrounding particles (Chang et al. 2007).

On the basis of our results and the findings of previous studies, incense emissions can be expected to pose a significant health risk if used regularly. This is partly due to the chemically complex nature of incense PM emissions. Chuang et al. (2011) found that the presence of multiple chemicals and metal(loids) on the surfaces of emitted incense particles was responsible for approximately 30% of oxidative DNA damage in the Plasmid Scission Test in comparison to nano-carbon black. In particular, it has been noted that the more water-soluble metals, such as As, Cd, Mn, and Ni, which have previously been identified in various brands of incense, are especially hazardous due to their increased bioavailability in comparison to water-insoluble metal(loid)s (See and Balasubramanian 2011). Yang et al. (2007) reported that the toxic equivalency value of solid-phase PAHs was 40-fold greater than the toxic equivalency value of gas-phase PAHs emitted by incense.

Another significant risk factor is the size of the emitted particles. Our finding that the peak particle size during incense burning was at 85 nm is concerning, given that particles of ≤ 100 nm (i.e., ultrafine particles) are most likely to be inhaled into the alveolar region of the lungs, where they pose the greatest risk to human health (See et al. 2007). At 1 h after completion of the burning period, the peak particle size only increased to approximately 110 nm. This finding indicates that a substantial proportion of ultrafine PM emissions may remain airborne and available for inhalation for significant periods of time after incense is burned. In one study investigating the respirable fraction of fine particles emitted from five different indoor household activities, the total lung deposition fraction of emitted incense particles was found to be 0.32 ± 0.03, of which 56.7–68.1% were found to be capable of depositing in the alveolar region of the lungs (Vu et al. 2017).

While in our investigation we focused on PM emissions from incense burning, this does not fully portray the human health risks of this activity. Harmful CO, NO_X, SO_2, VOCs (e.g., formaldehyde), and PAHs are also emitted, often at concentrations that exceed national and international ambient air quality guidelines (Cohen et al. 2013; Ho and Yu 2002; Jetter et al. 2002; Ji et al. 2010; Kuo and Tsai 2017; Kuo et al. 2016; Navasumrit et al. 2008; Yang et al. 2007). Furthermore, emitted gases were found in one study to decay over longer periods of time in comparison to PM (Cohen et al. 2013). Various measures can be taken to reduce exposure to incense PM and gas emissions, including the use of smokeless or short-burning incense, the selection of incense with non-toxic ingredients, and increasing ventilation to sites of incense burning (Chang et al. 2007; Cohen et al. 2013; Ji et al. 2010; Lung et al. 2003; See and Balasubramanian 2011; Yang et al. 2007). It should be noted that while smokeless incense releases fewer total particles (Yang et al. 2007), it has been found to release higher amounts of ultrafine particles in comparison to regular incense (See et al.

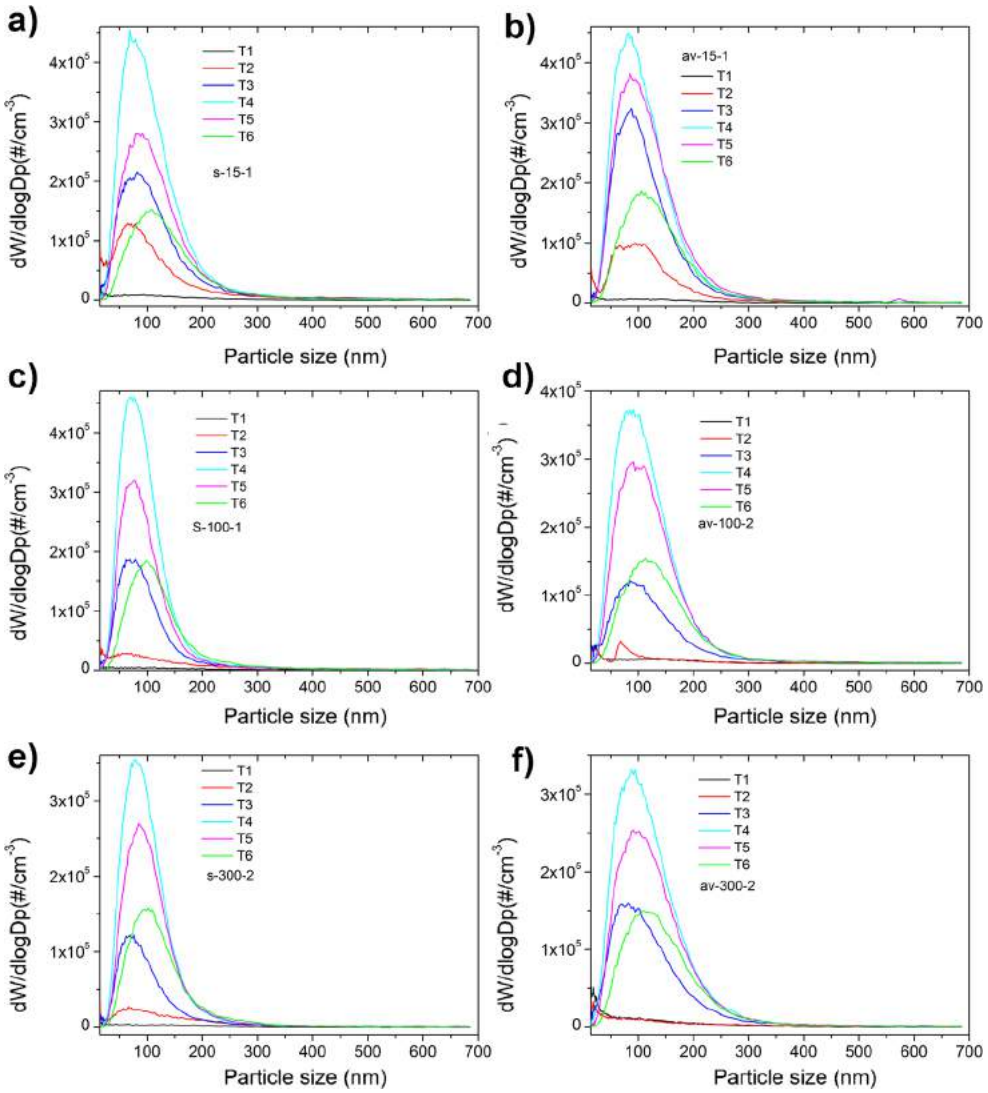

Fig. 8 Particle size distribution spectra for selected time points, including background prior to incense being lit (*T1*, black line), first measurement after the incense was lit (*T2*, red line), 15 min into the burning period (*T3*, blue line), burnout of the incense (*T4*, cyan line), 15 min after burnout (*T5*, pink line), and 1 h after burnout (*T6*, green). **a**, **c**, **e** correspond to "Strawbery" incense placed at 15 (*S-15-1*), 100 (*S-100-1*), and 300 (*S-300-2*) cm from the inlet, respectively; **b**, **d**), **f** correspond to "African Violet" incense placed at 15 (*AV-15-1*), 100 (*AV-100-2*), and 300 (*AV-300-2*) cm from the inlet, respectively

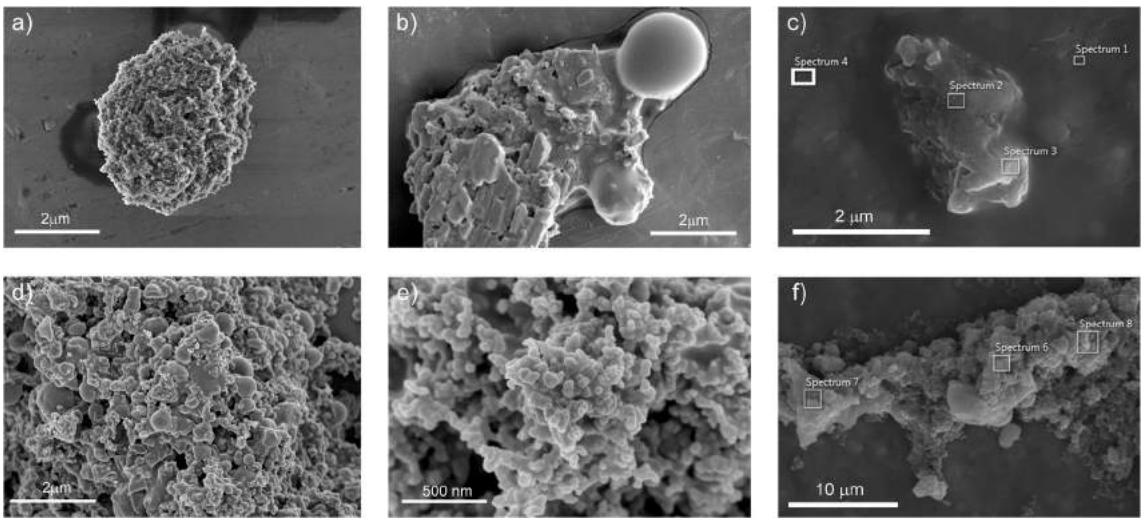

Fig. 9 Scanning electron microscopy images of "African Violet" incense particles collected with the Dekati® low-pressure cascade impactor (DLPI). **c**, **f** Representative images for the EDS analysis

Table 8 Energy dispersive X-ray spectroscopy analysis of "African Violet" incense corresponding to Fig. 9 c, f

Fig. 9c, f images[a]	C	O	Na	Mg	Al	Si	S	Cl	K	Ca	Fe
F9 C1	24.19				75.51						
F9 C2	70.28	12.83	0.17	0.21	13.83	0.69	0.20	0.35	0.08	0.84	0.30
F9 C3	46.28	35.42	1.60		9.02	6.05		0.09		0.96	0.26
F9 F6	58.96	29.32	1.62	0.76	2.03	0.36	1.15	0.46	4.20	0.56	
F9 F7	50.50	28.81	5.90	0.28	4.63	0.32	1.28	4.04	2.61	0.91	0.45
F9 F8	72.94	20.87	0.84	0.18	1.21	0.25	0.90	0.17	1.26	0.14	1.01

Values are given in atomic %

[a] F9 refers to Fig. 9; C1–C3 and F6–F8 refer to Fig. 9 part c, positions 1–3 and Fig. 9 part f, positions 6–8, respectively

2007). In another study, incenses marketed as 'environmentally friendly' were found to emit higher concentrations of PAHs and oxygenated PAHs compared to regular incenses (Lui et al. 2016) Therefore, incenses claiming to emit fewer pollutants should still be used with caution.

Conclusion

The emitted aerosol characteristics of two different types of incense were studied both before and after burning. The distribution of particle number and particle and concentrations were monitored at three different distances from the incense. At a distance of 100 cm from the measurement inlet, the first measurement of the nanoparticle concentration after the burning commenced showed a fourfold increase. The maximum concentration was obtained just before the incense burned out and was found to be 20- to 30-fold higher than the background particle concentrations. Even 100 min after the burning had concluded, particle concentrations were fourfold higher than the initial background concentrations. For the smallest nanoparticles measured (15 nm), the maximum concentration was obtained immediately upon lighting the incense, followed rapidly by a reduction, with the initial background levels reached shortly after. The peak nanoparticle concentration occurred for particles with diameters in the range of 60–100 nm. This finding reveals a high human health risk from burning incense since ultrafine particles (≤ 100 nm) are able to reach the alveolar region of the lungs, where the potential for harm is greatest. Analysis of the size-specific particle concentration by distance showed a decrease of nucleation mode particles with increasing distance from the measurement inlet.

The time evolution study of the TPC showed biexponential decay with two distinct lifetimes of several tens of minutes and > 100 min, respectively. These are attributed to the settling times for nucleation-mode particles with sizes of < 100 nm and to accumulation mode particles with sizes of up to 1μm. The particle size distribution spectra for different time points corresponding to the period just before the incense was lit, the first measurement after lighting the incense, and the measurement after the burnout were presented. These data show that while the concentration maximum remains at roughly the same diameter of the nanoparticle while the incense is burning, it shifts towards larger sizes after the burning is completed, indicating nanoparticle agglomeration during settling.

Chemical analyses and X-ray powder diffraction were performed and showed that the most abundant elements in the sample were C and Ca, with various amounts of H, Si, Al, and Fe. The main inorganic compounds in the sample were $CaCO_3$, CaO, and SiO_2. Additionally, the presence of some volatile organic compounds, such as nicotinic acid, cannot be excluded.

Our findings of high total particle concentrations during and following incense burning highlight the potential for prolonged exposure to air pollution during indoor incense burning under conditions of low ventilation. Countermeasures are recommended to minimize incense emission exposures by, for example, decreasing the burning time and increasing ventilation to the sites of incense burning.

Practical implications

The decay mechanisms of incense smoke in a room setting are presented. Emitted particles were found to have a long exposure in air, as significant concentrations were found even 100 min after the incense stick had completely burned out. Peak nanoparticle concentration occurred in the 60- to 100-nm range, making these particles a health hazard as they can reach the alveolar region of the lungs. The total nanoparticle concentration decayed biexponentially, with two lifetimes, namely, of several tens of minutes for particles up to 100 nm in diameter and longer than 100 min for particles with diameters of > 100 nm.

Acknowledgements This work has been partly financed and supported by the ISO-FOOD Project "ERA Chair for Isotope Techniques in Food Quality, Safety and Traceability" (grant agreement No. 621329) and Slovenian Research Agency, contract P1-0099. BV thanks Miri Trainic (Weizmann Institute of Science) for useful discussions.

Compliance with ethical standards

Conflict of interest The authors declare that they have no conflict of interest.

References

Bootdee S, Chantara S, Prapamontol T (2016) Determination of PM 2.5 and polycyclic aromatic hydrocarbons from incense burning emission at shrine for health risk assessment. Atmosph Poll Res 7:680–689

Brown JS, Zeman KL, Bennett WD (2002) Ultrafine particle deposition and clearance in the healthy and obstructed lung. Am J Respir Crit Care Med 166:1240–1247

Chang Y-C, Lee H-W, Tseng H-H (2007) The formation of incense smoke. J Aerosol Sci 38:39–51

Chen L-Y, Ho C (2016) Incense burning during pregnancy and birth weight and head circumference among term births. Taiwan Birth Cohort Stud Environ Health Perspect 124:1487

Chen Y, Ho W, Yu Y (2017) Adolescent lung function associated with incense burning and other environmental exposures at home. Indoor Air 27:746–752

Cheng Y, Bechtold W, Yu C, Hung I (1995) Incense smoke: characterization and dynamics in indoor environments. Aerosol Sci Technol 23: 271–281

Chuang H-C, Jones TP, Lung S-CC, BéruBé KA (2011) Soot-driven reactive oxygen species formation from incense burning. Sci Total Environ 409:4781–4787

Chuang H-C, BéruBé K, Lung S-CC, Bai K-J, Jones T (2013) Investigation into the oxidative potential generated by the formation of particulate matter from incense combustion. J Hazard Mater 244:142–150

Cohen R, Sexton KG, Yeatts KB (2013) Hazard assessment of United Arab Emirates (UAE) incense smoke. Sci Total Environ 458:176–186

Fang G-C, Chang C-N, Chu C-C, Wu Y-S, Fu PP-C, Chang S-C, Yang I-L (2003) Fine (PM 2.5), coarse (PM 2.5–10), and metallic elements of suspended particulates for incense burning at Tzu Yun yen temple in central. Taiwan Chemosph 51:983–991

Hayakawa R, Matsunaga K, Arima Y (1987) Depigmented contact dermatitis due to incense. Contact Dermatitis 16:272–274

Hinds WC (2012) Aerosol technology: properties, behavior, and measurement of airborne particles. Wiley, Hoboken

Ho SSH, Yu JZ (2002) Concentrations of formaldehyde and other carbonyls in environments affected by incense burning. J Environ Monit 4:728–733

European Commission (2015) Environment: Air Quality Standards [22.01.2015; 10.02.2015]. http://ec.europa.eu/environment/air/quality/standards.html

Huynh C, Savolainen H, Vu-Duc T, Guillemin M, Iselin F (1991) Impact of thermal proofing of a church on its indoor air quality: the combustion of candles and incense as a source of pollution. Sci Total Environ 102:241–251

Jetter JJ, Guo Z, McBrian JA, Flynn MR (2002) Characterization of emissions from burning incense. Sci Total Environ 295:51–67

Ji X, Le Bihan O, Ramalho O et al (2010) Characterization of particles emitted by incense burning in an experimental house. Indoor Air 20: 147–158

Kuo S-C, Tsai YI (2017) Emission characteristics of allergenic terpenols in PM 2.5 released from incense burning and the effect of light on the emissions. Sci Total Environ 584:495–504

Kuo S-C, Tsai YI, Sopajaree K (2016) Emission characteristics of carboxylates in PM 2.5 from incense burning with the effect of light on acetate. Atmos Environ 138:125–134

Lagzi I, Mészáros R, Gelybó G, Leelőssy Á (2013) Atmospheric chemistry. Eötvös Loránd University, Budapest

Lee S-C, Wang B (2004) Characteristics of emissions of air pollutants from burning of incense in a large environmental chamber. Atmos Environ 38:941–951

Lewinski N, Zhu H, Drezek R (2009) Evaluating strategies for risk assessment of nanomaterials nanotoxicity: from in vivo and in vitro models to health risks. Wiley, Chichester, pp 459–498

Lin T-C, Yang C-R, Chang F-H (2007) Burning characteristics and emission products related to metallic content in incense. J Hazard Mater 140:165–172

Löfroth G, Stensman C, Brandhorst-Satzkorn M (1991) Indoor sources of mutagenic aerosol particulate matter: smoking, cooking and incense burning. Mutat Res/Genet Toxicol 261:21–28

Lui K, Bandowe BAM, Ho SSH et al (2016) Characterization of chemical components and bioreactivity of fine particulate matter (PM 2.5) during incense burning. Environ Pollut 213:524–532

Lung SC, Kao MC, Hu SC (2003) Contribution of incense burning to indoor PM10 and particle-bound polycyclic aromatic hydrocarbons under two ventilation conditions. Indoor Air 13:194–199

Mannix RC, Nguyen KP, Tan EW, Ho EE, Phalen RF (1996) Physical characterization of incense aerosols. Sci Total Environ 193:149–158

Navasumrit P, Arayasiri M, Hiang OMT et al (2008) Potential health effects of exposure to carcinogenic compounds in incense smoke in temple workers. Chem Biol Interact 173:19–31

Nazaroff WW (2004) Indoor particle dynamics. Indoor Air 14:175–183

Nel A, Xia T, Mädler L, Li N (2006) Toxic potential of materials at the nanolevel. Science 311:622–627

Ott WR, Siegmann HC (2006) Using multiple continuous fine particle monitors to characterize tobacco, incense, candle, cooking, wood burning, and vehicular sources in indoor, outdoor, and in-transit settings. Atmos Environ 40:821–843

Remškar M, Tavčar G, Škapin SD (2015) Sparklers as a nanohazard: size distribution measurements of the nanoparticles released from sparklers. Air Qual Atmos Health 8:205–211

Rim D, Green M, Wallace L, Persily A, Choi J-I (2012) Evolution of ultrafine particle size distributions following indoor episodic releases: relative importance of coagulation, deposition and ventilation. Aerosol Sci Technol 46:494–503

See S, Balasubramanian R (2011) Characterization of fine particle emissions from incense burning. Build Environ 46:1074–1080

See SW, Balasubramanian R, Joshi UM (2007) Physical characteristics of nanoparticles emitted from incense smoke. Sci Technol Adv Mater 8:25–32

Song X, Ma W, Xu X et al (2017) The Association of Domestic Incense Burning with hypertension and blood pressure in Guangdong. Chi Int J Environ Res Publ Health 14:788

Stabile L, Fuoco F, Buonanno G (2012) Characteristics of particles and black carbon emitted by combustion of incenses, candles and anti-mosquito products. Build Environ 56:184–191

Vance ME, Marr LC (2015) Exposure to airborne engineered nanoparticles in the indoor environment. Atmos Environ 106:503–509

Vu TV, Ondracek J, Zdímal V, Schwarz J, Delgado-Saborit JM, Harrison RM (2017) Physical properties and lung deposition of particles emitted from five major indoor sources. Air Qual Atmos Health 10:1–14

Wang B, Lee S, Ho K (2006) Chemical composition of fine particles from incense burning in a large environmental chamber. Atmos Environ 40:7858–7868

Yang C-R, Lin T-C, Chang F-H (2006) Correlation between calcium carbonate content and emission characteristics of incense. J Air Waste Manage Assoc 56:1726–1732

Yang C-R, Lin T-C, Chang F-H (2007) Particle size distribution and PAH concentrations of incense smoke in a combustion chamber. Environ Pollut 145:606–615

Zhang Z, Chen Q (2006) Experimental measurements and numerical simulations of particle transport and distribution in ventilated rooms. Atmos Environ 40:3396–3408

Zhou R, An Q, Pan X, Yang B, Hu J, Wang Y (2015) Higher cytotoxicity and genotoxicity of burning incense than cigarette. Environ Chem Lett 13:465–471

Zhou Y, Deng Y, Wu P, Cao S-J (2017) The effects of ventilation and floor heating systems on the dispersion and deposition of fine particles in an enclosed environment. Build Environ 125:192–205

Zhuang C, Yang G, Long T, Hu D (2017) Numerical comparison of removal and deposition for fully-distributed particles in central-and split-type air-conditioning rooms. Build Environ 112:17–28